

Characterization of topological phase of superlattices in superconducting circuits

Jianfei Chen(陈健菲), Chaohua Wu(吴超华), Jingtao Fan(樊景涛), and Gang Chen(陈刚)
Citation: Chin. Phys. B, 2022, 31 (**8**): 088501. DOI: 10.1088/1674-1056/ac5612
Journal homepage: http://cpb.iphy.ac.cn; http://iopscience.iop.org/cpb

What follows is a list of articles you may be interested in

Shortcut-based quantum gates on superconducting qubits in circuit QED

Zheng-Yin Zhao(赵正印), Run-Ying Yan(闫润瑛), and Zhi-Bo Feng(冯志波)
Chin. Phys. B, 2021, 30 (**8**): 088501. DOI: 10.1088/1674-1056/abea96

Characteristics and mechanisms of subthreshold voltage hysteresis in 4H-SiC MOSFETs

Xi-Ming Chen(陈喜明), Bang-Bing Shi(石帮兵), Xuan Li(李轩), Huai-Yun Fan(范怀云), Chen-Zhan Li(李诚瞻), Xiao-Chuan Deng(邓小川), Hai-Hui Luo(罗海辉), Yu-Dong Wu(吴煜东), and Bo Zhang(张波)
Chin. Phys. B, 2021, 30 (**4**): 048504. DOI: 10.1088/1674-1056/abd391

Negative gate bias stress effects on conduction and low frequency noise characteristics in p-type poly-Si thin-film transistors

Chao-Yang Han(韩朝阳), Yuan Liu(刘远), Yu-Rong Liu(刘玉荣), Ya-Yi Chen(陈雅怡), Li Wang(王黎), Rong-Sheng Chen(陈荣盛)
Chin. Phys. B, 2019, 28 (**8**): 088502. DOI: 10.1088/1674-1056/28/8/088502

Influence of white light illumination on the performance of a-IGZO thin film transistor under positive gate-bias stress

Tang Lan-Feng, Yu Guang, Lu Hai, Wu Chen-Fei, Qian Hui-Min, Zhou Dong, Zhang Rong, Zheng You-Dou, Huang Xiao-Ming
Chin. Phys. B, 2015, 24 (**8**): 088504. DOI: 10.1088/1674-1056/24/8/088504

Low frequency noise and radiation response in the partially depleted SOI MOSFETs with ion implanted buried oxide

Liu Yuan, Chen Hai-Bo, Liu Yu-Rong, Wang Xin, En Yun-Fei, Li Bin, Lu Yu-Dong
Chin. Phys. B, 2015, 24 (**8**): 088503. DOI: 10.1088/1674-1056/24/8/088503

Characterization of topological phase of superlattices in superconducting circuits

Jianfei Chen(陈健菲)[1,2], Chaohua Wu(吴超华)[1,2,†], Jingtao Fan(樊景涛)[1,2], and Gang Chen(陈刚)[1,2,3]

[1] *State Key Laboratory of Quantum Optics and Quantum Optics Devices, Institute of Laser Spectroscopy, Shanxi University, Taiyuan* 030006, *China*
[2] *Collaborative Innovation Center of Extreme Optics, Shanxi University, Taiyuan* 030006, *China*
[3] *Collaborative Innovation Center of Light Manipulations and Applications, Shandong Normal University, Jinan* 250358, *China*

(Received 30 October 2021; revised manuscript received 14 February 2022; accepted manuscript online 17 February 2022)

The recent experimental observation of topological magnon insulator states in a superconducting circuit chain marks a breakthrough for topological physics with qubits, in which a dimerized qubit chain has been realized. Here, we extend such a dimer lattice to superlattice with arbitrary number of qubits in each unit cell in superconducting circuits, which exhibits rich topological properties. Specifically, by considering a quadrimeric superlattice, we show that the topological invariant (winding number) can be effectively characterized by the dynamics of the single-excitation quantum state through time-dependent quantities. Moreover, we explore the appearance and detection of the topological protected edge states in such a multiband qubit system. Finally, we also demonstrate the stable Bloch-like-oscillation of multiple interface states induced by the interference of them. Our proposal can be readily realized in experiment and may pave the way towards the investigation of topological quantum phases and topologically protected quantum information processing.

Keywords: superconducting circuits, topological phase transition, edge state, interface state

PACS: 85.25.–j, 03.67.Ac **DOI:** 10.1088/1674-1056/ac5612

1. Introduction

As one of the leading quantum platforms for implementing scalable quantum computation,[1–3] superconducting circuits have achieved great experimental progress in the past few years. In particular, due to the site-specific control and readout techniques, as well as the flexible and engineerable system designs,[4–6] a superconducting circuit system has emerged as a rich platform for quantum simulation.[7–10] By performing analog quantum simulations, a wide range of many-body physics has been employed in such simulators, such as the Bose–Hubbard model,[11–13] many-body localization,[14–18] quantum walks,[19–21] and dynamical phase transitions.[22] Moreover, due to the flexibility and diversity of superconducting quantum circuits system, it is also an excellent platform to realize exotic topological phases of matter and to probe and explore topologically protected effects, including the detection of topological invariant,[23] topological state transfer,[24,25] and higher-order topological phases.[26,27]

In a recent experiment,[28] topological magnon insulator states have been observed in a one-dimensional (1D) superconducting qubit chain with a tunable dimerized spin chain, which is analogue to the Su–Schrieffer–Heeger (SSH) model with two bands. Actually, various extended SSH models have been proposed to study novel topological physics by considering some other modulation terms, such as long range hoppings,[29] periodically driving,[30–32] and non-Hermitian modulation.[33–36] Recently, 1D superlattices with multiple sites (>2) in each unit cell have garnered much interest.[37–40] Such multiband systems show richer topological features than two-band models, such as the ability to tune the number of topological edge states by controlling the couplings, which allow one flexible control over the topological states in a new domain. Moreover, the superlattices with even sites in each unit cell preserve the chiral symmetry, and the topological phases can be characterized by the winding number.

In this work, we present an experimental feasible scheme to achieve the simulation of topological superlattice in a superconducting qubit chain with tunable coupling strengths. Such one-dimensional superlattices possess multiple topologically nontrivial dispersion bands and tunable edge states. Specifically, by considering a quadrimeric superlattice (SSH_4 model), we show that the topological invariant (winding number) can be effectively characterized by the dynamics of the single-excitation quantum state through an extended mean chiral displacement. Moreover, we explore the appearance and detection of the topological protected edge states in our qubit system. Finally, we also demonstrate the Bloch-oscillation-like dynamics induced by the interference of topological interface states with different propagation constants.

This article is organized as follows. Section 2 gives the feasible method to achieve one-dimensional superlattice in superconducting circuits. Section 3 demonstrates the measurement of topological winding number for quadrimeric lattice. Section 4 explores the existence and detection of topological edge states. Section 5 shows the dynamics of interface state propagation.

[†]Corresponding author. E-mail: sxwuchua@163.com

© 2022 Chinese Physical Society and IOP Publishing Ltd

2. Model and Hamiltonian

Based on the recent experiment,[28] we consider a one-dimensional spin chain consisting of N capacitively coupled qubits as shown in Fig. 1(a). The Hamiltonian of the system can be expressed as

$$\mathcal{H}=\sum_{j=0}^{N-1}\frac{\omega_j}{2}\sigma_j^+\sigma_j^-+\sum_{j=1}^{N-1}g_j\left(\sigma_{j-1}^++\sigma_{j-1}^-\right)\left(\sigma_j^++\sigma_j^-\right), \quad (1)$$

where σ_j^+ (σ_j^-) is the raising (lowering) operator of the jth qubit Q_j with transition frequency ω_j. The parameter g_j denotes the coupling strength between qubits Q_{j-1} and Q_j. In general, the coupling strengths are not adjustable. To achieve fully tunable coupling strengths, one can apply an ac magnetic flux to periodically modulate the qubit frequencies,[41,42]

$$\omega_j=\bar{\omega}_j+\varepsilon_j\sin\left(\nu_j t+\varphi_j\right), \quad (2)$$

where $\bar{\omega}_j$ is the mean operating frequency, ε_j, ν_j, and φ_j are the modulation amplitude, frequency, and phase respectively. By defining a rotating frame $U=U_1\times U_2$ with

$$U_1=\exp\left[-\mathrm{i}\left(\sum_{j=0}^{N-1}\frac{\bar{\omega}_j}{2}\sigma_j^z\right)t\right], \quad (3)$$

$$U_2=\exp\left[\mathrm{i}\sum_{j=0}^{N-1}\sigma_j^z\frac{\alpha_j}{2}\cos\left(\nu_j t+\varphi_j\right)\right], \quad (4)$$

where $\alpha_j=\varepsilon_j/\nu_j$, we can obtain the transformed Hamiltonian

$$\begin{aligned}\mathcal{H}_{\mathrm{I}} &= \mathrm{i}\frac{\mathrm{d}U^\dagger}{\mathrm{d}t}U+U^\dagger HU\\ &=\sum_{j=1}^{N-1}g_j\left\{\sigma_{j-1}^+\sigma_j^-\,\mathrm{e}^{\mathrm{i}\Delta_j t}\exp\left[-\mathrm{i}\alpha_{j-1}\cos\left(\nu_{j-1}t+\varphi_{j-1}\right)\right]\right.\\ &\quad\left.\exp\left[\mathrm{i}\alpha_j\cos\left(\nu_j t+\varphi_j\right)\right]+\mathrm{H.c.}\right\}, \quad (5)\end{aligned}$$

where $\Delta_j=\bar{\omega}_j-\bar{\omega}_{j-1}$. We consider $\Delta_j=\nu_j\,(-\nu_j)$ for odd (even) j.[41] Then, using the Jacobi–Anger identity

$$\exp\left[\mathrm{i}\alpha\cos\left(\nu t+\varphi\right)\right]=\sum_{l=-\infty}^{\infty}\mathrm{i}^l\mathcal{J}_l\left(\alpha\right)\mathrm{e}^{\mathrm{i}l\left(\nu t+\varphi\right)}, \quad (6)$$

with $\mathcal{J}_l\left(\alpha\right)$ being the lth Bessel function of the first kind, and applying the rotating-wave approximation by neglecting the high-order oscillation terms, the effective Hamiltonian becomes

$$\mathcal{H}_{\mathrm{eff}}=\sum_{j=1}^{N-1}g_j'\sigma_{j-1}^+\sigma_j^-+\mathrm{H.c.}, \quad (7)$$

with the effective coupling strength

$$g_j'=g_j\mathcal{J}_1\left(\alpha_j\right)\mathcal{J}_0\left(\alpha_{j-1}\right)\mathrm{e}^{\pm\mathrm{i}\left(\varphi_j\pm\pi/2\right)}, \quad (8)$$

where $\pm$ denotes j being odd and even in g_j', respectively. From Eq. (8), it is clear that the coupling strength g_j' can be conveniently tuned independently by changing $\alpha_j=\varepsilon_j/\nu_j$. Moreover, there is a phase factor in each coupling which is derived from the driving phase φ_j. Such a superconducting qubit chain with tunable couplings can be used to study quantum state transfer,[43] quantum gate,[44] and gauge potentials.[45] Moreover, we can realize generalized superlattice in addition to the simple SSH model in such a qubit chain with fully tunable couplings.

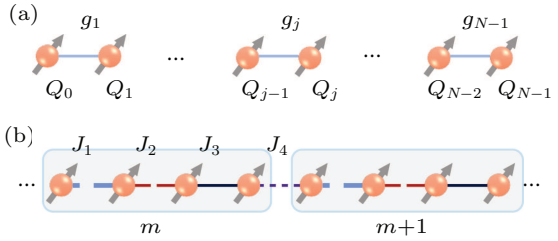


Fig. 1. (a) Schematic diagram of a qubit chain. Here, Q_j denotes the jth qubit, g_j is the coupling between neighboring qubits. (b) Schematic diagram of a quadrimeric superlattice with four qubits in each unit cell. J_1, J_2, and J_3 are the intra-cell couplings, whereas J_4 is the inter-cell coupling.

To demonstrate the topological properties of superlattice in superconducting circuits, here we focus on a superlattice qubit chain with four qubits in each unit cell denoted as $\{1,2,3,4\}$, as shown in Fig. 1(b), which is known as the SSH$_4$ model. For such a quadrimeric lattice, the Hamiltonian reads

$$\begin{aligned}H &= \sum_{m=1}^{M}\left(J_1\sigma_{m,1}^+\sigma_{m,2}^-+J_2\sigma_{m,2}^+\sigma_{m,3}^-+J_3\sigma_{m,3}^+\sigma_{m,4}^-\right.\\ &\quad\left.+J_4\sigma_{m,4}^+\sigma_{m+1,1}^-+\mathrm{H.c.}\right), \quad (9)\end{aligned}$$

where m is the unit cell index, M is the number of the unit cells, J_1, J_2, and J_3 denote the intracell qubit coupling strengths and J_4 is the intercell qubit coupling strength. For simplicity, we take $\hbar=1$ and set J_1 as the energy scale.

Note that the Hamiltonian (9) describes an interacting spin chain. Here, we consider the single-excitation case, i.e., one of the qubits is excited to the excited state $|e\rangle$ and the others stay in the ground state $|g\rangle$.

3. Topological phase transition

To study the topological feature of the qubit superlattice, we rewrite the Hamiltonian (9) in the momentum space as

$$\tilde{H}\left(k\right)=\begin{pmatrix}0 & h^\dagger\\ h & 0\end{pmatrix}=\begin{pmatrix}0 & 0 & J_1 & J_4\,\mathrm{e}^{-\mathrm{i}k}\\ 0 & 0 & J_2 & J_3\\ J_1 & J_2 & 0 & 0\\ J_4\,\mathrm{e}^{\mathrm{i}k} & J_3 & 0 & 0\end{pmatrix}. \quad (10)$$

The eigenvalues are given by $E=\pm\sqrt{\left(J\pm\sqrt{J^2-4T}\right)/2}$ with $J=J_1^2+J_2^2+J_3^2+J_4^2$ and $T=(J_1J_3)^2+(J_2J_4)^2-2J_1J_2J_3J_4\cos k$. It is found that there are four bands. If $J_1J_3=\pm J_2J_4$, the gap between the middle bands is closed at $k=0$ or $k=\pi$.

By introducing the matrix $\Gamma = I_2 \otimes \sigma_z$ with I_2 being the 2×2 identity matrix, one can verify that $\Gamma\tilde{H} + \tilde{H}\Gamma = 0$. Therefore, the SSH_4 model has a chiral symmetry and belongs to the same class of the SSH model, and the corresponding winding number can be obtained as follows:

$$w = \frac{1}{2\pi \mathrm{i}} \int_0^{2\pi} \mathrm{d}k z^{-1} \frac{\mathrm{d}z}{\mathrm{d}k}, \tag{11}$$

where $z = \det(h) = J_1 J_3 - J_2 J_4 \mathrm{e}^{\mathrm{i}k}$. Through a straightforward calculation, we have

$$w = \begin{cases} 1, & |J_1 J_3| < |J_2 J_4|, \\ 0, & |J_1 J_3| > |J_2 J_4|. \end{cases} \tag{12}$$

The winding number $w = 1$ (0) shows that the above qubit chain [Eq. (9)] is in the topologically nontrivial (trivial) phase.

For one-dimensional chiral symmetric systems, the winding number is an important topological invariant used to characterize the topological phase and can be measured through the dynamics of quantum state. That is, the winding number can be extracted from a time-dependent quantity–mean chiral displacement (MCD), which has been measured experimentally in cold atoms,[46] photonic system,[47] and superconducting qubit chain for the SSH-type model.[28] For the SSH_4-type qubit chain, we define the chiral displacement operator as (see the appendix)

$$\hat{\mathcal{C}} = \sum_x x(\hat{P}^{\mathrm{e}}_{1x} - \hat{P}^{\mathrm{e}}_{2x} + \hat{P}^{\mathrm{e}}_{3x} - \hat{P}^{\mathrm{e}}_{4x}), \tag{13}$$

with $\hat{P}^{\mathrm{e}}_{ix} = |e\rangle_{ix}\langle e|$ $(i = 1,2,3,4)$. Here, x is the relabeled unit cell index with $\{x = \cdots, -1, 0, 1, \cdots\}$. Then the dynamics of the MCD is given as $\mathcal{C}(t) = \langle\psi(t)|\hat{\mathcal{C}}|\psi(t)\rangle$. Here, $|\psi(t)\rangle = \mathrm{e}^{-\mathrm{i}\hat{H}t}|\psi(0)\rangle$ with $|\psi(0)\rangle$ being the initial state at time $t = 0$. The long-time average of the MCD, i.e., $\bar{\mathcal{C}} = \lim_{T\to\infty} 1/T \int_0^T \mathrm{d}t\mathcal{C}(t)$ can be used to characterize topological invariant.

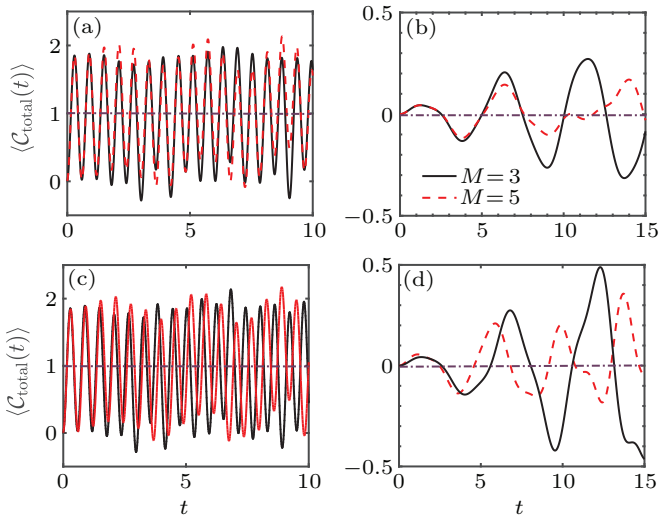


Fig. 2. (a) and (b) The dynamics of $\mathcal{C}_{\mathrm{total}}(t)$ with $J_4 = 5$ (a) and $J_4 = 0.2$ (b), respectively. (c) and (d) The dynamics of $\langle\mathcal{C}_{\mathrm{total}}(t)\rangle$ with $J_4 = 5$ (c) and $J_4 = 0.2$ (d), respectively. Here, $\langle\cdots\rangle$ denotes the disorder-averaged $\mathcal{C}_{\mathrm{total}}(t)$. The other parameters are chosen as $J_1 = J_2 = J_3$ and $W = 0.2$.

In order to detect the winding number for the SSH_4-type qubit chain, we consider two single excitation initial states localized on the central unit cell, i.e., $|\psi_1(0)\rangle = |gggg,\ldots,eggg,\ldots,gggg\rangle$ and $|\psi_3(0)\rangle = |gggg,\ldots,ggeg,\ldots,gggg\rangle$. The corresponding MCDs are denoted as $\mathcal{C}_1(t)$ and $\mathcal{C}_3(t)$, respectively. The topological winding number can be extracted from the total MCD–$\mathcal{C}_{\mathrm{total}}(t) = \mathcal{C}_1(t) + \mathcal{C}_3(t)$, that is,

$$w = \bar{\mathcal{C}}_{\mathrm{total}}. \tag{14}$$

As shown in Figs. 2(a) and 2(b), we simulate $\mathcal{C}_{\mathrm{total}}(t)$ for different configurations with $J_4 > J_1 (= J_2 = J_3)$ and $J_4 < J_1 (= J_2 = J_3)$, corresponding to topological non-trivial and trivial phases, respectively. It is clear that the curve of $\mathcal{C}_{\mathrm{total}}(t)$ oscillates around 1 when $J_4 > J_1$, which gives the topological winding number $w = 1$. For $J_4 < J_1$, $\mathcal{C}_{\mathrm{total}}(t)$ oscillates around the average values 0 corresponding to trivial phase with $w = 0$. These results show that the long time dynamics of the chiral operator [Eq. (13)] can be effectively characterized different topological phases for SSH_4-type qubit chain.

To demonstrate the robustness of the MCD, we add the disorder to each qubit couplings as $J_i^{\mathrm{m}} = J_i + W\delta$, where W is the disorder strength and $\delta \in [-0.5, 0.5]$ is a random number. In Figs. 2(c) and 2(d), we show the disorder-averaged MCD $\langle\mathcal{C}_{\mathrm{total}}\rangle$ by averaging $\mathcal{C}_{\mathrm{total}}(t)$ over 30 independent disorder configurations for trivial and nontrivial phases. It can be seen that $\langle\mathcal{C}_{\mathrm{total}}\rangle$ is robust to the weak disorder, maintaining oscillation center around 1 and 0 for $J_4 > J_1$ and $J_4 < J_1$, respectively.

4. Detecting of edge states

A hallmark feature of topological insulators is the topologically protected boundary states. For the two-band SSH model, it supports limited number (one or two) of topological edge states. However, the superlattice systems show richer topological features due to the multiple topologically nontrivial dispersion bands. To determine the existence of topological phases and edge states, it is convenient to analyze the symmetries of the Hamiltonian. For Hamiltonian (10), the system possesses inversion symmetry, i.e., $\mathcal{P}H(k)\mathcal{P}^{-1} = H(-k)$ with $\mathcal{P} = \sigma_x \otimes \sigma_x$ when $J_1 = J_3$. Figure 4(a) shows the energy spectrum with $J_1 = J_3$. It is clear that there are two zero-energy degenerate edge states in the middle gap for $J_4 > J_{4,0}$ $(= J_1 J_3/J_2)$, and there are two degenerate edge states for $J_4 > J_{4,1}$ $(= J_2)$ in the upper and lower gaps. Such topological phases can be described by the Zak phase, which is defined as $\gamma_s = \mathrm{i}\int_{-\pi}^{\pi} \mathrm{d}k \langle\psi_{s,k}|\partial_k\psi_{s,k}\rangle$ with $\psi_{s,k}$ being the sth-Bloch-wave functions. For multiband systems, the topological properties of the nth band gap is characterized by the sum of Zak

phase of all the isolated bands below the corresponding band gap, i.e.,

$$\mathcal{Z}_n = \gamma_1 + \cdots + \gamma_n. \tag{15}$$

In Figs. 3(a1)–3(a3), we plot the Zak phase $\mathcal{Z}_n$ $(n = 1,2,3)$ of the corresponding band gap of the SSH_4 model under the inversion symmetry. We find that $\mathcal{Z}_n$ is quantized and can take the values zero or π, denoting the trivial and nontrivial topological phases, respectively. The nontrivial Zak phase implies that a pair of topologically protected edge states will appear at the boundaries of the system.

In the case of $J_1 \neq J_3$, the superlattice has no inversion symmetry. Figure 3(b) shows the energy spectrum and Figs. 3(b1)–3(b3) show the corresponding gap Zak phase $\mathcal{Z}_n$ with $J_1 \neq J_3$. It can be seen that the Zak phase of the middle gap is quantized, and a pair of degenerate zero-energy edge state emerge for $J_4 > J_{4,2}$ $(= J_1 J_3 / J_2)$. However, for the upper and lower gaps, the Zak phases $\mathcal{Z}_{1,3}$ are not quantized and vary continuously. The non-degenerate edge states emerge without experiencing a gap closing and reopening point, and they are not topological.

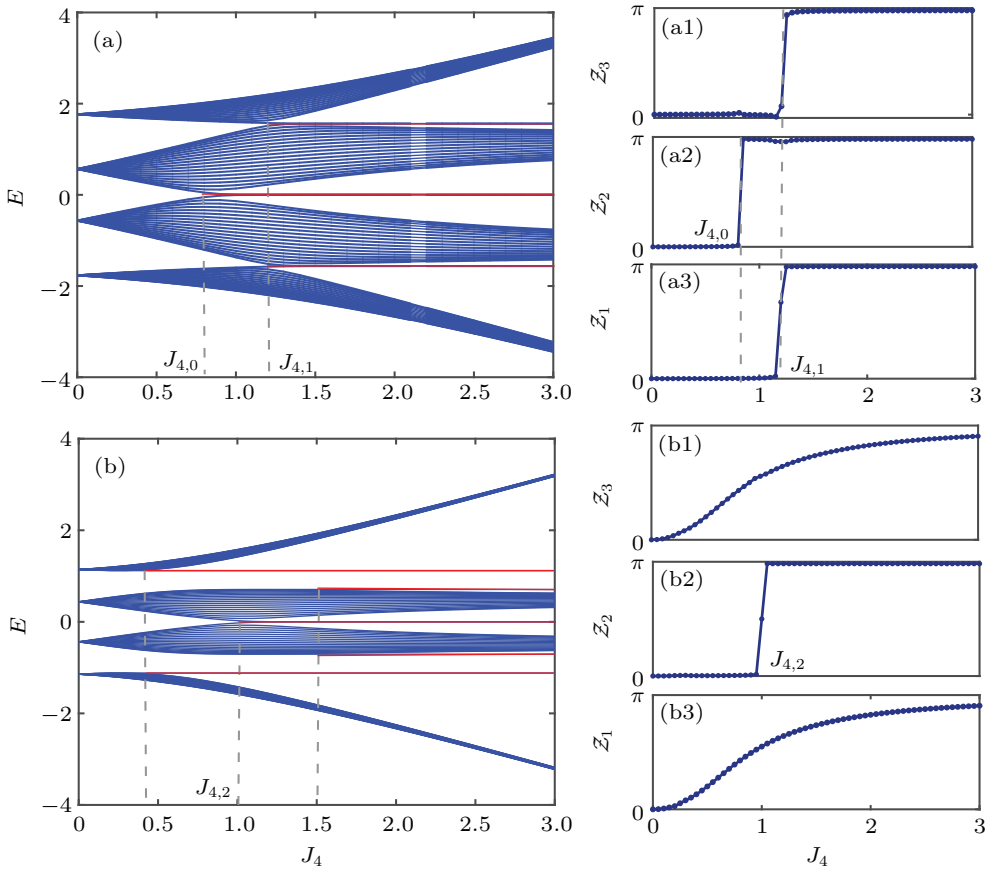


Fig. 3. (a) The energy spectrum with the inversion symmetry $\{J_1 = J_3 = 1, J_2 = 1.2\}$. (a1)–(a3) The corresponding band gap Zak phases $\mathcal{Z}_n$ versus the inter-cell coupling J_4. (b) The energy spectrum without inversion symmetry $\{J_1 = 1, J_3 = 0.5, J_2 = 0.5\}$. (b1)–(b3) The Zak phases corresponding to all band gaps.

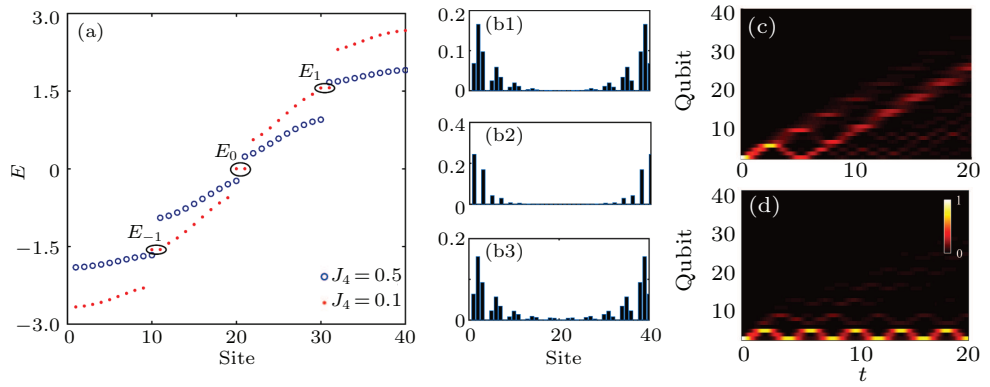


Fig. 4. (a) The energy spectrum with $J_4 = 0.5$ (blue circle) and $J_4 = 2$ (red dot). (b1)–(b3) The distribution of wave functions of the three pairs edge states indicated by circles in (a), respectively. (c) and (d) The time evolution of the single-excited state population for $J_4 = 0.5$ (a) and $J_4 = 2$ (b), respectively. The other parameters are chosen as $J_1 = J_3 = 1$ and $J_2 = 1.2$.

The above discussion shows that the number of topological edge states can be controlled by tuning the inter- and intracell couplings. The topological edge states can be detected by the dynamics of the single-excitation quantum state. As an example, in Fig. 4(a), we plot the energy spectrum with $J_4 = 0.5$ (blue circle) and $J_4 = 2$ (red dot). In the topological phase ($J_4 = 2$), there are three pairs of edge state in the gaps and the distribution wave functions of them are shown in Figs. 4(b1)–4(b3). Figures 4(c) and 4(d) show the time evolution of the single-excited state ($|\psi(0)\rangle = \sigma_1^+ |G\rangle$) population for $J_4 = 0.5$ and $J_4 = 2$, respectively. For the non-topological phase, the excited state spreads into the bulk over time, while in the topological phase with edge states, the wave-packet remains localized around the boundary unit cell.

5. Dynamics of interface state

Another important topological aspect is the existence of interface states between two topological distinct insulators. As shown schematically in Fig. 5(a), a topological interface (shaded region) can be created by combining two SSH_4-type qubit systems with different topological properties [e.g., in Fig. 5(a), the qubit array on the right (left) represents a topologically nontrivial (trivial) array with $J_4 < J_1 = J_2 = J_3$ ($J_4 > J_1 = J_2 = J_3$)]. The energy spectrum is sown in Fig. 5(b) with $\{J_{1,2,3} = 1, J_4 = 5\}$. There are three localized interface states existing in the gap, and the distribution of these three states are shown in Fig. 5(c).

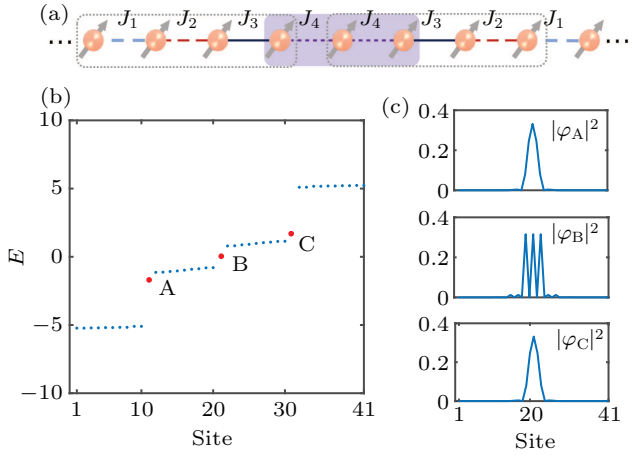


Fig. 5. (a) Schematic diagram of the two-coupled-qubit chain with different topological phases. The central shaded region denotes the interface. (b) The energy spectrum of the qubit configuration shown in (a). The red dots represent the interface states. (c) The distribution wave function of the interface states. The parameters are chosen are $J_1 = J_2 = J_3$, $J_4 = 5$ and $M = 10$.

To observe the dynamics of topological interface states, we excite the central qubit of the interface region [Fig. 5(a)]. Such an initial state has a large overlap with the wave function of the interface states and it will propagate in the qubit chain via the interface states. Compared with the localized defect state in the SSH-type qubit chain, the interface states of superlattice exhibit exotic behaviors.[37,39] Figures 6(a) and 6(b) show the time evolutions of single-excitation state population with $M = 4$ and $M = 2$, respectively. It is found that the dynamics of the single-excitation exhibits Bloch-like oscillation. Such breathing-like oscillation is due to the interference of topological interface states with different propagation constants, which is quite different from general Bloch oscillation with a linear potential.[48] The results indeed indicate that the single-excited state is localized in the center interface region of the qubit chain, unambiguously demonstrate the existence of the topological interface states.

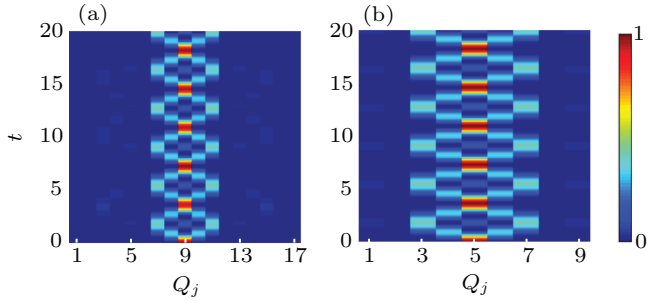


Fig. 6. Time evolutions of all qubit's excited state population with $M = 4$ (a) and $M = 2$ (b). The initial excitation is the central qubit of the interface region as shown in Fig. 5(a). The other parameters are the same as those in Fig. 5(b).

6. Conclusion

In summary, we have constructed one-dimensional superlattices in superconducting circuits with tunable coupling strengths. As an example, we consider the quadrimeric lattice. Such a multiband system shows richer topological properties than the dimeric case. Through the non-equilibrium dynamics of a single-qubit excitation state, we show that the topological winding number can be measured by a dynamical dependent quantity, i.e., mean chiral displacement, which takes zero for the trivial phase and 1 for the nontrivial phase. Moreover, we have demonstrated the existence of topological edge state under different parameters region. Finally, the stable Bloch-like oscillation of multiple interface states induced by the interference of them has been demonstrated. In the experiment, accurate single-shot readout techniques enable us to synchronously record the dynamics of all qubits and to observe the evolution of a single-excitation state. In addition, the physics presented here persists even for finite size, indicating the feasibility of experimental measurements. Note that similar physics can be extended to superlattices with arbitrary number of qubits in each unit cell. Our work potentially paves the way for exploring novel topological states of matter in controllable superconducting circuits.

Appendix A

Here, we derive the validity of the mean chiral displacement in our quarimeric lattice.[49] First, let us define the projectors $P_j = |\psi_j\rangle\langle\psi_j|$ and $Q = \sum_{j=1,2} Q_j = \sum_{j=1,2}(P_j - P_{-j})$,

where $|\psi_j\rangle$ ($j=\pm1,\pm2$) denotes the the eigenstate of the Bloch Hamiltonian (10) with energy E_j. These representations comes from the chiral symmetry where the eigenenergies and eigenstates satisfy $E_j=-E_{-j}$ and $\hat{\Gamma}|\psi_j\rangle=|\psi_{-j}\rangle$. The winding number can be computed through the integral over the Brillouin zone of the skew polarization $S=\sum_{j\in\text{occ}}S_j$, i.e., $w=\oint\frac{\mathrm{d}k}{\pi}S(k)$, where $S_j=\mathrm{i}\left\langle\Gamma\psi_j|\psi'_j\right\rangle$ with $\left|\psi'_j\right\rangle=\partial_k|\psi_j\rangle$.

For a generic localized state $\overline{|\Psi\rangle}$, the mean chiral displacement ($\langle\hat{\mathcal{C}}(t)\rangle\equiv\left\langle\hat{\Gamma}\cdot x(t)\right\rangle$) is given by

$$\left\langle\hat{\Gamma}\cdot x(t)\right\rangle_{\bar{\Psi}}=\oint\sum_{j=1,2}\frac{\mathrm{d}k}{2\pi}\langle\Psi|U_t^{\dagger}\Gamma\left(i\partial_k\right)U_t|\Psi\rangle, \tag{A1}$$

where $U_t=\mathrm{e}^{-\mathrm{i}Ht}$ is the unitary evolution operator and $\overline{|\Psi\rangle}=\oint\frac{\mathrm{d}k}{2\pi}|\Psi\rangle$. Through a simple calculation, we have

$$\begin{aligned}
&P_j\left[U^{-t}\Gamma\partial_kU^t\right]P_{j'}\\
&=\delta_{j,-j'}\left[P_j\Gamma\partial_k\frac{\mathrm{e}^{\mathrm{i}2tE_j}}{2}+\mathrm{e}^{\mathrm{i}2tE_j}|\psi_j\rangle\langle\psi'_{-j}|\right]\\
&\quad+\mathrm{e}^{\mathrm{i}t(E_j-E_{j'})}|\psi_j\rangle\left\langle\psi_{-j}|\psi'_{j'}\right\rangle\langle\psi_{j'}|\\
&=\delta_{j,-j'}\left[P_j\Gamma\partial_k\frac{\mathrm{e}^{\mathrm{i}2tE_j}}{2}+\mathrm{e}^{\mathrm{i}2tE_j}|\psi_j\rangle\langle\psi'_{-j}|\right]\\
&\quad-\mathrm{e}^{\mathrm{i}t(E_j-E_{j'})}|\psi_j\rangle\langle\psi'_{-j}|P_{j'}.
\end{aligned}\tag{A2}$$

For simplicity, we define the projector on the subspace of chiral-partner eigenstates, $R_j=P_j+P_{-j}$. Equation (A2) multiplied by i gives the sum of two terms, a term T_1 which acts in the subspace of chiral partner states with $|j|=|j'|$ and a term T_2 which acts in the subspace of the states with $|j|\neq|j'|$. Using $R_j\Gamma=\Gamma_j$, $\partial_k\Gamma=0$ and $\mathrm{i}Q_jS_j=\partial_k\left(Q_j\Gamma\right)/2$, these two terms become

$$\begin{aligned}
T_1&=\sum_{j=1}^{D/2}S_j\left[1-\cos\left(2E_jt\right)\right]R_j+iR_j\Gamma\partial_k\left[\frac{\cos\left(2E_jt\right)}{2}\right]\\
&\quad-Q_j\Gamma\partial_k\left[\frac{\sin\left(2E_jt\right)}{2}\right]-\mathrm{i}Q_jS_j\sin\left(2E_jt\right)\\
&=\sum_{j=1}^{D/2}S_j\left[1-\cos\left(2E_jt\right)\right]R_j\\
&\quad+\partial_k\left[\mathrm{i}\Gamma_j\frac{\cos\left(2E_jt\right)}{2}-Q_j\Gamma\frac{\sin\left(2E_jt\right)}{2}\right],
\end{aligned}\tag{A3}$$

$$T_2=\sum_{j,j'=\pm1,\pm2\,(|j|\neq|j'|)}\left\langle\psi_{-j}|\psi'_{j'}\right\rangle|\psi_j\rangle\langle\psi_{j'}|\,\mathrm{e}^{\mathrm{i}t(E_j-E_{j'})}. \tag{A4}$$

It is obvious that the term T_2 is purely oscillatory, so it will average to zero in the long time limit. Considering $\langle\Gamma\rangle_{\psi_j}=0$ and $\langle Q\Gamma\rangle_{\psi_j}=0$, we have

$$\left\langle\hat{\Gamma}\cdot x\left(t\right)\right\rangle_{\bar{\Psi}}=\oint\frac{\mathrm{d}k}{2\pi}\left\langle T_2+\sum_{j=1,2}S_j[1-\cos(2tE_j)]R_j\right\rangle_{\Psi}. \tag{A5}$$

For the state $\overline{|\psi_j\rangle}$ ($=\oint\frac{\mathrm{d}k}{2\pi}|\psi_j\rangle$) and $\overline{|\Gamma_j\rangle}$ ($=[\mathrm{sgn}(j)\overline{|\psi_j\rangle}+\overline{|\psi_{-j}\rangle}/\sqrt{2}]$), we have $\langle T_2\rangle_{\psi_j}=\langle T_2\rangle_{\Gamma_j}=0$ and $\langle R_j\rangle_{\psi_{j'}}=\langle R_j\rangle_{\Gamma_{j'}}=\delta_{jj'}$, then obtain

$$\begin{aligned}
\sum_{j=1,2}\left\langle\hat{\Gamma}\cdot x\right\rangle_{\bar{\Gamma}_j}&=\sum_{j=1,2}\left\langle\hat{\Gamma}\cdot x\right\rangle_{\bar{\Psi}_j}\\
&=\oint\frac{\mathrm{d}k}{2\pi}\sum_{j=1}^{D/2}S_j[1-\cos(2tE_j)]\\
&=\frac{w}{2}+\text{osc.},
\end{aligned}\tag{A6}$$

where osc. denotes the oscillatory term which tends to zero in the long time limit.

Acknowledgements

Project supported by the National Natural Science Foundation of China (Grant Nos. 12034012, 12074232,12125406, and 11804204) and 1331KSC.

References

[1] Koch J, Yu T M, Gambetta J, Houck A A, Schuster D I, Majer J, Blais A, Devoret M H, Girvin S M and Schoelkopf R J 2007 *Phys. Rev. A* **76** 042319

[2] Gu X, Kockum A F, Miranowicz A, Liu Y and Nori F 2017 *Phys. Rep.* **718** 1

[3] Blais A, Grimsmo A L, Girvin S M and Wallraff A 2021 *Rev. Mod. Phys.* **93** 025005

[4] Wang Z, Bao Z, Wu Y, Li Y, Ma C, Cai T, Song Y, Zhang H and Duan L 2021 *Chin. Phys. Lett.* **38** 110303

[5] Li D Y, Chu J, Zheng W, Lan D, Zhao J, Li S X, Tan X S and Yu Y 2021 *Chin. Phys. B* **30** 070308

[6] Ye Y, Cao S, Wu Y, Chen X, Zhu Q, Li S, Chen F, Gong M, Zha C, Huang H L, Zhao Y, Wang S, Guo S, Qian H, Liang F, Lin J, Xu Y, Guo C, Sun L, Li N, Deng H, Zhu X and Pan J W 2021 *Chin. Phys. Lett.* **38** 100301

[7] Houck A A, Tüeci H E and Koch J 2012 *Nat. Phys.* **8** 292

[8] Georgescu I M, Ashhab S and Nori F 2014 *Rev. Mod. Phys.* **86** 153

[9] Xue Z Y and Hu Y 2021 *Adv. Quantum Technol.* **4** 2100017

[10] He K, Geng X, Huang R, Liu J and Chen W 2021 *Chin. Phys. B* **30** 080304

[11] Jin J, Rossini D, Fazio R, Leib M and Hartmann M J 2013 *Phys. Rev. Lett.* **110** 163605

[12] Ye Y, Ge Z Y, Wu Y, Wang S, Gong M, Zhang Y R, Zhu Q, Yang R, Li S, Liang F, Lin J, Xu Y, Guo C, Sun L, Cheng C, Ma N, Meng Z Y, Deng H, Rong H, Lu C Y, Peng C Z, Fan H, Zhu X and Pan J W 2019 *Phys. Rev. Lett.* **123** 050502

[13] Kounalakis M, Dickel C, Bruno A, Langford N K and Steele G A 2018 *npj Quantum Inf.* **4** 38

[14] Roushan P, *et al.* 2017 *Science* **358** 1175

[15] Xu K, Chen J J, Zeng Y, Zhang Y R, Song C, Liu W, Guo Q, Zhang P, Xu D, Deng H, Huang K, Wang H, Zhu X, Zheng D and Fan H 2018 *Phys. Rev. Lett.* **120** 050507

[16] Orell T, Michailidis A A, Serbyn M and Silveri M 2019 *Phys. Rev. B* **100** 134504

[17] Guo Q, Cheng C, Sun Z H, Song Z, Li H, Wang Z, Ren W, Dong H, Zheng D, Zhang Y R, Mondaini R, Fan H and Wang H 2021 *Nat. Phys.* **17** 234

[18] Gong M, Neto G D, Zha C, Wu Y, Rong H, Ye Y, Li S, Zhu Q, Wang S, Zhao Y, Liang F, Lin J, Xu Y, Peng C Z, Deng H, Bayat A, Zhu X and Pan J W 2021 *Phys. Rev. Res.* **3** 033043

[19] Gong M, Wang S, Zha C, Chen M C, Huang H L, Wu Y, Zhu Q, Zhao Y, Li S, Guo S, Qian H, Ye Y, Chen F, Ying C, Yu J, Fan D, Wu D, Su H, Deng H, Rong H, Zhang K, Cao S, Lin J, Xu Y, Sun L, Guo C, Li N, Liang F, Bastidas V M, Nemoto K, Munro W J, Huo Y H, Lu C Y, Peng C Z, Zhu X and Pan J W 2021 *Science* **372** 948

[20] Yan Z, Zhang Y R, Gong M, Wu Y, Zheng Y, Li S, Wang C, Liang F, Lin J, Xu Y, Guo C, Sun L, Peng C Z, Xia K, Deng H, Rong H, You J Q, Nori F, Fan H, Zhu X and Pan J W 2019 *Science* **364** 753

[21] Flurin E, Ramasesh V V, Hacohen-Gourgy S, Martin L S, Yao N Y and Siddiqi I 2017 *Phys. Rev. X* **7** 031023

[22] Xu K, Sun Z, Liu W, Zhang Y R, Li H, Dong H, Ren W, Zhang P, Nori F, Zheng D, Fan H and Wang H 2020 *Sci. Adv.* **6** eaba4935

[23] Ramasesh V V, Flurin E, Rudner M, Siddiqi I and Yao N Y 2017 *Phys. Rev. Lett.* **118** 130501

[24] Mei F, Chen G, Tian L, Zhu S L and Jia S 2018 *Phys. Rev. A* **98** 012331

[25] Hu K X, Chen C, Qi L, Cui W X, Zhang S and Wang H F 2021 *Phys. Rev. A* **104** 023707

[26] Wu C, Guan X, Fan J, Chen G and Jia S 2021 *Phys. Rev. A* **104** 022601

[27] Niu J, Yan T, Zhou Y, Tao Z, Li X, Liu W, Zhang L, Liu S, Yan Z, Chen Y and Yu D 2021 *Sci. Bull.* **66** 1168

[28] Cai W, Han J, Mei F, Xu Y, Ma Y, Li X, Wang H, Song Y P, Xue Z Y, Yin Z Q, Jia S and Sun L 2019 *Phys. Rev. Lett.* **123** 080501

[29] Li L, Xu Z and Chen S 2014 *Phys. Rev. B* **89** 085111

[30] Bandyopadhyay S, Bhattacharya U and Dutta A 2019 *Phys. Rev. B* **100** 054305

[31] Vyas V M and Roy D 2021 *Phys. Rev. B* **103** 075441

[32] Bandyopadhyay S and Dutta A 2019 *Phys. Rev. B* **100** 144302

[33] Liu J S, Han Y Z and Liu C S 2019 *Chin. Phys. B* **28** 100304

[34] Liu J S, Han Y Z and Liu C S 2020 *Chin. Phys. B* **29** 010302

[35] Yao S and Wang Z 2018 *Phys. Rev. Lett.* **121** 086803

[36] Wang X R, Guo C X, Du Q and Kou S P 2020 *Chin. Phys. Lett.* **37** 117303

[37] Midya B and Feng L 2018 *Phys. Rev. A* **98** 043838

[38] Xie D, Gou W and Xiao T 2019 *npj Quantum Inf.* **5** 55

[39] Wang Y, Lu Y H, Gao J, Chang Y J, Tang H and Jin X M 2019 *Phys. Rev. B* **103** 014110

[40] Stefano L 2019 *Opt. Lett.* **44** 2530

[41] Li X, Ma Y, Han J, Chen T, Xu Y, Cai W, Wang H, Song Y P, Xue Z Y, Yin Z Q and Sun L 2018 *Phys. Rev. Appl.* **10** 054009

[42] Reagor M, Osborn C, Tezak N, *et al.* 2018 *Sci. Adv.* **4** eaao3603

[43] Li J W, Wu C W and Dai H Y 2011 *Chin. Phys. Lett.* **28** 090302

[44] Chen T, Shen P and Xue Z Y 2020 *Phys. Rev. Applied* **14** 034038

[45] Guan X, Feng Y L, Xue Z Y, Chen G and Jia S 2020 *Phys. Rev. A* **102** 032610

[46] Meier E J, An F A, Dauphin A, Maffei M, Massignan P, Hughes T L and Gadway B 2018 *Science* **362** 929

[47] Cardano F, D'Errico A, Dauphin A, Maffei M, Piccirillo B, Lisio C D, Filippis G D, Cataudella V, Santamato E, Marrucci L, Lewenstein M and Massignan P 2017 *Nat. Commun.* **8** 15516

[48] Guo X Y, Ge Z Y, Li H, Wang Z, Zhang Y R, Song P, Xiang Z, Song X, Jin Y, Lu L, Xu K, Zheng D and Fan H 2021 *npj Quantum Inf.* **7** 51

[49] Maffei M, Dauphin A, Cardano F, Lewenstein M and Massignan P 2018 *New J. Phys.* **20** 013023